

Quantum Backaction on kg-Scale Mirrors: Observation of Radiation Pressure Noise in the Advanced Virgo Detector

F. Acernese,^{1,2} M. Agathos,³ L. Aiello,^{4,5} A. Ain,^{6,7} A. Allocca,⁶ A. Amato,⁸ S. Ansoldi,^{9,10} S. Antier,¹¹ M. Arène,¹¹ N. Arnaud,^{12,13} S. Ascenzi,^{4,14} P. Astone,¹⁵ F. Aubin,¹⁶ S. Babak,¹¹ F. Badaracco,^{4,5} M. K. M. Bader,¹⁷ S. Bagnasco,¹⁸ J. Baird,¹¹ G. Ballardin,¹³ G. Baltus,¹⁹ C. Barbieri,^{20,21,22} P. Barneo,²³ F. Barone,^{24,2} M. Barsuglia,¹¹ D. Barta,²⁵ A. Basti,^{7,6} M. Bawaj,^{26,27} M. Bazzan,^{28,29} M. Bejger,³⁰ I. Belahcene,¹² S. Bernuzzi,³ D. Bersanetti,³¹ A. Bertolini,¹⁷ M. Bischì,^{32,33} M. Bitossi,^{13,6} M.-A. Bizouard,³⁴ O. Blanch,³⁵ F. Bobba,^{36,37} M. Boer,³⁴ G. Bogaert,³⁴ M. Boldrini,^{38,15} F. Bondu,³⁹ R. Bonnand,¹⁶ B. A. Boom,¹⁷ V. Boschi,⁶ V. Boudart,¹⁹ Y. Bouffanais,^{28,29} A. Bozzi,¹³ C. Bradaschia,⁶ M. Branchesi,^{4,5} M. Breschi,³ T. Briant,⁴⁰ F. Brighenti,^{32,33} A. Brillet,³⁴ J. Brooks,¹³ G. Bruno,⁴¹ T. Bulik,⁴² H. J. Bulten,^{17,43} D. Buskulic,¹⁶ G. Cagnoli,⁸ E. Calloni,^{44,2} M. Canepa,^{45,31} G. Carapella,^{36,37} F. Carbognani,¹³ M. Carpinelli,^{46,47} G. Carullo,^{7,6} J. Casanueva Diaz,¹³ C. Casentini,^{48,14} S. Caudill,¹⁷ F. Cavalier,¹² R. Cavalieri,¹³ G. Cella,⁶ P. Cerdá-Durán,⁴⁹ E. Cesarini,¹⁴ W. Chaibi,³⁴ P. Chanial,¹³ E. Chassande-Mottin,¹¹ F. Chiadini,^{50,37} R. Chierici,⁵¹ A. Chincarini,³¹ A. Chiummo,¹³ N. Christensen,³⁴ S. Chua,⁴⁰ G. Ciani,^{28,29} P. Ciecielag,³⁰ M. Cieřlar,³⁰ M. Cifaldi,^{48,14} R. Ciolfi,^{52,29} F. Cipriano,³⁴ A. Cirone,^{45,31} S. Clesse,⁴¹ F. Cleva,³⁴ E. Coccia,^{4,5} P.-F. Cohadon,⁴⁰ D. E. Cohen,¹² M. Colpi,^{20,21} L. Conti,²⁹ I. Cordero-Carión,⁵³ S. Corezzi,^{27,26} D. Corre,¹² S. Cortese,¹³ J.-P. Coulon,³⁴ M. Croquette,⁴⁰ J. R. Cudell,¹⁹ E. Cuoco,^{13,54} M. Curylo,⁴² B. D'Angelo,^{45,31} S. D'Antonio,¹⁴ L. D'Onofrio,^{44,2} D. D'Urso,^{46,47} T. Dal Canton,¹² V. Dattilo,¹³ M. Davier,¹² M. De Laurentis,^{44,2} F. De Matteis,^{48,14} R. De Pietri,^{55,56} R. De Rosa,^{44,2} C. De Rossi,¹³ J. Degallaix,⁵⁷ W. Del Pozzo,^{7,6} S. Deléglise,⁴⁰ A. Depasse,⁴¹ L. Di Fiore,² C. Di Giorgio,^{36,37} F. Di Giovanni,⁴⁹ M. Di Giovanni,^{58,59} T. Di Girolamo,^{44,2} A. Di Lieto,^{7,6} S. Di Pace,^{38,15} I. Di Palma,^{38,15} F. Di Renzo,^{7,6} T. Dietrich,¹⁷ M. Drago,^{4,5} J.-G. Ducoin,¹² O. Durante,^{36,37} P.-A. Duverne,¹² M. Eisenmann,¹⁶ L. Errico,^{44,2} D. Estevez,¹⁶ V. Fafone,^{48,14,4} S. Farinon,³¹ M. Fays,¹⁹ F. Feng,¹¹ E. Fenyvesi,^{25,60} I. Ferrante,^{7,6} F. Fidecaro,^{7,6} P. Figura,⁴² I. Fiori,¹³ D. Fiorucci,^{4,5} R. Fittipaldi,^{61,37} V. Fiumara,^{62,37} R. Flaminio,^{16,63} J. A. Font,^{49,64} J.-D. Fournier,³⁴ S. Frasca,^{38,15} F. Frasconi,⁶ V. Frey,¹² G. G. Fronzè,¹⁸ R. Gamba,³ B. Garaventa,^{31,45} F. Garufi,^{44,2} G. Gemme,³¹ A. Gennai,⁶ Archisman Ghosh,^{17,65,66,67} B. Giacomazzo,^{20,21,22} L. Giacoppo,^{38,15} P. Giri,^{6,7} M. Gosselin,^{7,6} R. Gouaty,¹⁶ A. Grado,^{68,2} M. Granata,⁵⁷ V. Granata,³⁶ G. Greco,^{32,33} G. Grignani,^{27,26} A. Grimaldi,^{58,59} S. J. Grimm,^{4,5} P. Gruning,¹² G. M. Guidi,^{32,33} G. Guixé,²³ Y. Guo,¹⁷ P. Gupta,^{17,69} L. Haegel,¹¹ O. Halim,^{5,4} O. Hannuksela,^{69,17} T. Harder,³⁴ K. Haris,^{17,69} J. Harms,^{4,5} A. Heidmann,⁴⁰ H. Heitmann,³⁴ P. Hello,¹² G. Hemming,¹³ E. Hennes,¹⁷ D. Hofman,⁵⁷ V. Hui,¹⁶ B. Idzkowski,⁴² A. Iess,^{48,14} G. Intini,^{38,15} T. Jacqmin,⁴⁰ K. Janssens,⁷⁰ P. Jaranowski,⁷¹ R. J. G. Jonker,¹⁷ C. Karathanasis,³⁵ S. Katsanevas,¹³ F. Kéfélian,³⁴ I. Khan,^{4,14} N. Khetan,^{4,5} G. Koekoek,^{17,72} S. Koley,¹⁷ M. Kolstein,³⁵ A. Królak,^{73,74} I. La Rosa,¹⁶ D. Laghi,^{7,6} A. Lamberts,^{34,75} A. Lartaux-Vollard,¹² C. Lazzaro,^{29,28} P. Leaci,^{38,15} N. Leroy,¹² N. Letendre,¹⁶ F. Linde,^{76,17} M. Llorens-Monteagudo,⁴⁹ A. Longo,^{77,78} M. Lorenzini,^{48,14} V. Loriette,⁷⁹ G. Losurdo,⁶ D. Lumaca,^{48,14} A. Macquet,³⁴ C. Magazzù,⁶ E. Majorana,¹⁵ I. Maksimovic,⁷⁹ N. Man,³⁴ V. Mangano,^{38,15} M. Mantovani,¹³ M. Mapelli,^{28,29} F. Marchesoni,^{80,26} F. Marion,¹⁶ A. Marquina,⁵³ S. Marsat,¹¹ F. Martelli,^{32,33} M. Martinez,³⁵ V. Martinez,⁸ A. Masserot,¹⁶ S. Mastrogiovanni,¹¹ A. Menendez-Vazquez,³⁵ L. Mereni,⁵⁷ M. Merzougui,³⁴ R. Metzdrorf,⁴⁰ A. Miani,^{58,59} C. Michel,⁵⁷ L. Milano,^{44,2} A. Miller,⁴¹ E. Milotti,^{81,10} O. Minazzoli,^{34,82} Y. Minenkov,¹⁴ Ll. M. Mir,³⁵ M. Montani,^{32,33} F. Morawski,³⁰ B. Mours,⁸³ F. Muciaccia,^{38,15} A. Nagar,^{84,18,85} I. Nardecchia,^{48,14} L. Naticchioni,¹⁵ J. Neilson,^{86,37} G. Nelemans,⁸⁷ C. Nguyen,¹¹ S. Nissanke,^{65,17} F. Nocera,¹³ G. Oganessian,^{4,5} C. Olivetto,¹³ G. Pagano,^{7,6} G. Pagliaroli,^{4,5} C. Palomba,¹⁵ T. H. Pang,^{17,69} F. Pannarale,^{38,15} F. Paoletti,⁶ A. Paoli,¹³ A. Paolone,^{15,88} D. Pascucci,¹⁷ A. Pasqualetti,¹³ R. Passaquieti,^{7,6} D. Passuello,⁶ B. Patricelli,^{7,6} M. Pegoraro,²⁹ A. Perego,^{58,59} C. Périgois,¹⁶ A. Perreca,^{58,59} S. Perriès,⁵¹ K. S. Phukon,^{17,76} O. J. Piccinni,^{38,15} M. Pichot,³⁴ M. Piendibene,^{7,6} F. Piergiovanni,^{32,33} L. Pierini,^{38,15} V. Pierro,^{86,37} G. Pillant,¹³ F. Pilo,⁶ L. Pinard,⁵⁷ I. M. Pinto,^{86,37,84} K. Piotrzkowski,⁴¹ E. Placidi,³⁸ W. Plastino,^{77,78,89} R. Poggiani,^{7,6} E. Polini,¹⁶ P. Popolizio,¹³ E. K. Porter,¹¹ M. Pracchia,¹⁶ M. Principe,^{86,84,37} G. A. Prodi,^{90,59} P. Proposito,^{48,14} A. Puecher,^{17,69} M. Punturo,²⁶ F. Puosi,^{6,7} P. Puppò,¹⁵ G. Raaijmakers,^{65,17} N. Radulesco,³⁴ P. Rapagnani,^{38,15} M. Razzano,^{7,6} T. Regimbau,¹⁶ L. Rei,³¹ P. Rettengo,^{91,18} F. Ricci,^{38,15} G. Riemenschneider,^{91,18} F. Robinet,¹² A. Rocchi,¹⁴ L. Rolland,¹⁶ M. Romanelli,³⁹ R. Romano,^{1,2} A. Romero,³⁵ S. Ronchini,^{4,5} D. Rosińska,⁴² P. Ruggi,¹³ O. S. Salafia,^{22,21,20} L. Salconi,¹³ A. Samajdar,^{17,69} N. Sanchis-Gual,⁹² E. Santos,³⁴ B. Sassolas,⁵⁷ O. Sauter,¹⁶ S. Sayah,⁵⁷ M. Seglar-Arroyo,¹⁶ D. Sentenac,¹³ V. Sequino,^{44,2} A. Sharma,^{4,5} M. Sieniawska,³⁰ N. Singh,⁴² A. Singhal,^{4,15} V. Sipala,^{46,47} V. Sordini,⁵¹ F. Sorrentino,³¹ N. Sorrentino,^{7,6} R. Soulard,³⁴ M. Spera,^{28,29} C. Stachie,³⁴ D. A. Steer,¹¹ G. Stratta,^{93,33} A. Sur,³⁰ B. L. Swinkels,¹⁷ M. Tacca,¹⁷

A. J. Tanasijczuk,⁴¹ E. N. Tapia San Martin,¹⁷ M. Tonelli,^{7,6} A. Torres-Forné,⁹⁴ I. Tosta e Melo,^{46,47} A. Trapananti,^{80,26}
 F. Travasso,^{26,80} M. C. Tringali,⁴² A. Trovato,¹¹ K. W. Tsang,^{17,95,69} M. Turconi,³⁴ M. Valentini,^{58,59} N. van Bakel,¹⁷
 M. van Beuzekom,¹⁷ J. F. J. van den Brand,^{72,43,17} C. Van Den Broeck,^{69,17} L. van der Schaaf,¹⁷ M. Vardaro,^{76,17}
 M. Vasúth,²⁵ G. Vedovato,²⁹ D. Verkindt,¹⁶ F. Vetrano,³² A. Viceré,^{32,33} J.-Y. Vinet,³⁴ H. Vocca,^{27,26} R. C. Walet,¹⁷ M. Was,¹⁶
 A. Zadrożny,⁷⁴ T. Zelenova,¹³ and J.-P. Zendri²⁹

(The Virgo Collaboration)

¹*Dipartimento di Farmacia, Università di Salerno, I-84084 Fisciano, Salerno, Italy*

²*INFN, Sezione di Napoli, Complesso Universitario di Monte S. Angelo, I-80126 Napoli, Italy*

³*Theoretisch-Physikalisches Institut, Friedrich-Schiller-Universität Jena, D-07743 Jena, Germany*

⁴*Gran Sasso Science Institute (GSSI), I-67100 LAquila, Italy*

⁵*INFN, Laboratori Nazionali del Gran Sasso, I-67100 Assergi, Italy*

⁶*INFN, Sezione di Pisa, I-56127 Pisa, Italy*

⁷*Università di Pisa, I-56127 Pisa, Italy*

⁸*Université de Lyon, Université Claude Bernard Lyon 1, CNRS, Institut Lumière Matière, F-69622 Villeurbanne, France*

⁹*Dipartimento di Matematica e Informatica, Università di Udine, I-33100 Udine, Italy*

¹⁰*INFN, Sezione di Trieste, I-34127 Trieste, Italy*

¹¹*Université de Paris, CNRS, Astroparticule et Cosmologie, F-75013 Paris, France*

¹²*Université Paris-Saclay, CNRS/IN2P3, IJCLab, 91405 Orsay, France*

¹³*European Gravitational Observatory (EGO), I-56021 Cascina, Pisa, Italy*

¹⁴*INFN, Sezione di Roma Tor Vergata, I-00133 Roma, Italy*

¹⁵*INFN, Sezione di Roma, I-00185 Roma, Italy*

¹⁶*Laboratoire d'Annecy de Physique des Particules (LAPP), Université Grenoble Alpes, Université Savoie Mont Blanc, CNRS/IN2P3, F-74941 Annecy, France*

¹⁷*Nikhef, Science Park 105, 1098 XG Amsterdam, Netherlands*

¹⁸*INFN Sezione di Torino, I-10125 Torino, Italy*

¹⁹*Université de Liège, B-4000 Liège, Belgium*

²⁰*Università degli Studi di Milano-Bicocca, I-20126 Milano, Italy*

²¹*INFN, Sezione di Milano-Bicocca, I-20126 Milano, Italy*

²²*INAF, Osservatorio Astronomico di Brera sede di Merate, I-23807 Merate, Lecco, Italy*

²³*Institut de Ciències del Cosmos, Universitat de Barcelona, C/ Martí i Franquès 1, Barcelona, 08028, Spain*

²⁴*Dipartimento di Medicina, Chirurgia e Odontoiatria Scuola Medica Salernitana, Università di Salerno, I-84081 Baronissi, Salerno, Italy*

²⁵*Wigner RCP, RMKI, H-1121 Budapest, Konkoly Thege Miklós út 29-33, Hungary*

²⁶*INFN, Sezione di Perugia, I-06123 Perugia, Italy*

²⁷*Università di Perugia, I-06123 Perugia, Italy*

²⁸*Università di Padova, Dipartimento di Fisica e Astronomia, I-35131 Padova, Italy*

²⁹*INFN, Sezione di Padova, I-35131 Padova, Italy*

³⁰*Nicolaus Copernicus Astronomical Center, Polish Academy of Sciences, 00-716, Warsaw, Poland*

³¹*INFN, Sezione di Genova, I-16146 Genova, Italy*

³²*Università degli Studi di Urbino Carlo Bo, I-61029 Urbino, Italy*

³³*INFN, Sezione di Firenze, I-50019 Sesto Fiorentino, Firenze, Italy*

³⁴*Artemis, Université Côte d'Azur, Observatoire Côte d'Azur, CNRS, F-06304 Nice, France*

³⁵*Institut de Física d'Altes Energies (IFAE), Barcelona Institute of Science and Technology, and ICREA, E-08193 Barcelona, Spain*

³⁶*Dipartimento di Fisica E.R. Caianiello, Università di Salerno, I-84084 Fisciano, Salerno, Italy*

³⁷*INFN, Sezione di Napoli, Gruppo Collegato di Salerno, Complesso Universitario di Monte S. Angelo, I-80126 Napoli, Italy*

³⁸*Università di Roma La Sapienza, I-00185 Roma, Italy*

³⁹*Université de Rennes, CNRS, Institut FOTON—UMR6082, F-3500 Rennes, France*

⁴⁰*Laboratoire Kastler Brossel, Sorbonne Université, CNRS, ENS-Université PSL, Collège de France, F-75005 Paris, France*

⁴¹*Université catholique de Louvain, B-1348 Louvain-la-Neuve, Belgium*

⁴²*Astronomical Observatory Warsaw University, 00-478 Warsaw, Poland*

⁴³*VU University Amsterdam, 1081 HV Amsterdam, Netherlands*

⁴⁴*Università di Napoli Federico II, Complesso Universitario di Monte S. Angelo, I-80126 Napoli, Italy*

⁴⁵*Dipartimento di Fisica, Università degli Studi di Genova, I-16146 Genova, Italy*

⁴⁶*Università degli Studi di Sassari, I-07100 Sassari, Italy*

⁴⁷*INFN, Laboratori Nazionali del Sud, I-95125 Catania, Italy*

- ⁴⁸*Università di Roma Tor Vergata, I-00133 Roma, Italy*
- ⁴⁹*Departamento de Astronomía y Astrofísica, Universitat de València, E-46100 Burjassot, València, Spain*
- ⁵⁰*Dipartimento di Ingegneria Industriale (DIIN), Università di Salerno, I-84084 Fisciano, Salerno, Italy*
- ⁵¹*Institut de Physique des 2 Infinis de Lyon, CNRS/IN2P3, Université de Lyon, Université Claude Bernard Lyon 1, F-69622 Villeurbanne, France*
- ⁵²*INAF, Osservatorio Astronomico di Padova, I-35122 Padova, Italy*
- ⁵³*Departamento de Matemáticas, Universitat de València, E-46100 Burjassot, València, Spain*
- ⁵⁴*Scuola Normale Superiore, Piazza dei Cavalieri, 7—56126 Pisa, Italy*
- ⁵⁵*Dipartimento di Scienze Matematiche, Fisiche e Informatiche, Università di Parma, I-43124 Parma, Italy*
- ⁵⁶*INFN, Sezione di Milano Bicocca, Gruppo Collegato di Parma, I-43124 Parma, Italy*
- ⁵⁷*Laboratoire des Matériaux Avancés (LMA), Institut de Physique des 2 Infinis de Lyon, CNRS/IN2P3, Université de Lyon, F-69622 Villeurbanne, France*
- ⁵⁸*Università di Trento, Dipartimento di Fisica, I-38123 Povo, Trento, Italy*
- ⁵⁹*INFN, Trento Institute for Fundamental Physics and Applications, I-38123 Povo, Trento, Italy*
- ⁶⁰*Institute for Nuclear Research, Hungarian Academy of Sciences, Bem t'er 18/c, H-4026 Debrecen, Hungary*
- ⁶¹*CNR-SPIN, c/o Università di Salerno, I-84084 Fisciano, Salerno, Italy*
- ⁶²*Scuola di Ingegneria, Università della Basilicata, I-85100 Potenza, Italy*
- ⁶³*National Astronomical Observatory of Japan, 2-21-1 Osawa, Mitaka, Tokyo 181-8588, Japan*
- ⁶⁴*Osservatori Astronomic, Universitat de València, E-46980 Paterna, València, Spain*
- ⁶⁵*GRAPPA, Anton Pannekoek Institute for Astronomy and Institute for High-Energy Physics, University of Amsterdam, Science Park 904, 1098 XH Amsterdam, Netherlands*
- ⁶⁶*Delta Institute for Theoretical Physics, Science Park 904, 1090 GL Amsterdam, Netherlands*
- ⁶⁷*Lorentz Institute, Leiden University, Niels Bohrweg 2, 2333 CA Leiden, Netherlands*
- ⁶⁸*INAF, Osservatorio Astronomico di Capodimonte, I-80131 Napoli, Italy*
- ⁶⁹*Department of Physics, Utrecht University, Princetonplein 1, 3584 CC Utrecht, Netherlands*
- ⁷⁰*Universiteit Antwerpen, Prinsstraat 13, 2000 Antwerpen, Belgium*
- ⁷¹*University of Bialystok, 15-424 Bialystok, Poland*
- ⁷²*Maastricht University, P.O. Box 616, 6200 MD Maastricht, Netherlands*
- ⁷³*Institute of Mathematics, Polish Academy of Sciences, 00656 Warsaw, Poland*
- ⁷⁴*National Center for Nuclear Research, 05-400 wierk-Otwock, Poland*
- ⁷⁵*Laboratoire Lagrange, Université Côte d'Azur, Observatoire Côte d'Azur, CNRS, F-06304 Nice, France*
- ⁷⁶*Institute for High-Energy Physics, University of Amsterdam, Science Park 904, 1098 XH Amsterdam, Netherlands*
- ⁷⁷*Dipartimento di Matematica e Fisica, Università degli Studi Roma Tre, I-00146 Roma, Italy*
- ⁷⁸*INFN, Sezione di Roma Tre, I-00146 Roma, Italy*
- ⁷⁹*ESPCI, CNRS, F-75005 Paris, France*
- ⁸⁰*Università di Camerino, Dipartimento di Fisica, I-62032 Camerino, Italy*
- ⁸¹*Dipartimento di Fisica, Università di Trieste, I-34127 Trieste, Italy*
- ⁸²*Centre Scientifique de Monaco, 8 quai Antoine 1er, MC-98000, Monaco*
- ⁸³*Institut Pluridisciplinaire Hubert CURIE, 23 rue du loess—BP28 67037 Strasbourg cedex 2, France*
- ⁸⁴*Museo Storico della Fisica e Centro Studi e Ricerche Enrico Fermi, I-00184 Roma, Italy*
- ⁸⁵*Institut des Hautes Etudes Scientifiques, F-91440 Bures-sur-Yvette, France*
- ⁸⁶*Dipartimento di Ingegneria, Università del Sannio, I-82100 Benevento, Italy*
- ⁸⁷*Department of Astrophysics/IMAPP, Radboud University Nijmegen, P.O. Box 9010, 6500 GL Nijmegen, Netherlands*
- ⁸⁸*Consiglio Nazionale delle Ricerche—Istituto dei Sistemi Complessi, Piazzale Aldo Moro 5, I-00185 Roma, Italy*
- ⁸⁹*Accademia Nazionale dei Lincei—Centro Linceo Interdisciplinare “Beniamino Segre”, Palazzo Corsini, Via della Lungara, 10, I-00165 Rome, Italy*
- ⁹⁰*Università di Trento, Dipartimento di Matematica, I-38123 Povo, Trento, Italy*
- ⁹¹*Dipartimento di Fisica, Università degli Studi di Torino, I-10125 Torino, Italy*
- ⁹²*Centro de Astrofísica e Gravitação (CENTRA), Departamento de Física, Instituto Superior Técnico, Universidade de Lisboa, 1049-001 Lisboa, Portugal*
- ⁹³*INAF, Osservatorio di Astrofisica e Scienza dello Spazio, I-40129 Bologna, Italy*
- ⁹⁴*Max Planck Institute for Gravitationalphysik (Albert Einstein Institute), D-14476 Potsdam-Golm, Germany*
- ⁹⁵*Van Swinderen Institute for Particle Physics and Gravity, University of Groningen, Nijenborgh 4, 9747 AG Groningen, Netherlands*

M. Mehmet, H. Vahlbruch, H. Lück, and K. Danzmann
*Institut für Gravitationsphysik, Leibniz Universität Hannover and
 Max-Planck-Institut für Gravitationsphysik (Albert-Einstein-Institut), Callinstr. 38, 30167 Hannover, Germany*

 (Received 1 May 2020; revised 22 June 2020; accepted 27 July 2020; published 22 September 2020)

The quantum radiation pressure and the quantum shot noise in laser-interferometric gravitational wave detectors constitute a macroscopic manifestation of the Heisenberg inequality. If quantum shot noise can be easily observed, the observation of quantum radiation pressure noise has been elusive, so far, due to the technical noise competing with quantum effects. Here, we discuss the evidence of quantum radiation pressure noise in the Advanced Virgo gravitational wave detector. In our experiment, we inject squeezed vacuum states of light into the interferometer in order to manipulate the quantum backaction on the 42 kg mirrors and observe the corresponding quantum noise driven displacement at frequencies between 30 and 70 Hz. The experimental data, obtained in various interferometer configurations, is tested against the Advanced Virgo detector quantum noise model which confirmed the measured magnitude of quantum radiation pressure noise.

DOI: [10.1103/PhysRevLett.125.131101](https://doi.org/10.1103/PhysRevLett.125.131101)

Introduction.—Current interferometric gravitational wave detectors (GWDs) are the most sensitive devices for measuring differential length changes. Advanced Virgo [1], Advanced LIGO [2], GEO600 [3], and KAGRA [4] are kilometer-scale Michelson-type interferometers that use high power laser systems to probe changes of the distance between suspended test masses at the level of 10^{-19} m/ $\sqrt{\text{Hz}}$. The precision of any continuous position measurement is bound by a quantum limit enforced by the Heisenberg inequality which constrains the uncertainty with which two noncommuting variables can be observed. As found by Braginsky [5] and Caves [6] several decades ago, the implication of this quantum mechanical limit for GWDs (operating at frequencies between a few tens of Hz and kHz) is the existence of two noises limiting the detectors sensitivity, both originating from vacuum fluctuations entering the dark (antisymmetric) port of the interferometer: quantum shot noise (QSN) and quantum radiation pressure noise (QRPN). As also described in [6], the quantum noise limited sensitivity of a GWD can be enhanced via the injection of squeezed vacuum states of light, and this technique has been successfully demonstrated to reduce the QSN in gravitational wave detectors [7–9]. While QSN has been observed for decades in GWDs and, also, reduced using squeezing techniques, QRPN has not been observed so far due to other noise sources competing with quantum effects.

In order to demonstrate the observation of QRPN, one of the main experimental issues is the ratio of QRPN to Brownian thermal noise. Therefore, it comes as no surprise that the first demonstration of QRPN was performed with a ng-scale optomechanical membrane probed by laser light [10], embedded in a 4-K cryostat and further cooled by radiation pressure to a temperature in the mK range. QRPN

close to the mechanical resonance was also observed with microwave illumination of a drum resonator embedded in a microwave cavity [11]. Recent experiments extended such observations further away from mechanical resonances in the free mass regime, either with an optomechanical resonator with ultralow dissipation [12] or a 70 μm mirror suspended from a single-crystal 55 μm long GaAs cantilever [13]. The manipulation of QRPN with squeezed light has been demonstrated in the microwave [14] and optical [15] domains.

Here, we present the observation of QRPN on the 42 kg mirrors of the Advanced Virgo detector. The measured mirrors displacement noise induced by the backaction force fluctuations scales with the level of injected squeezing according to the interferometer quantum noise model. For large squeezing values, the low frequency noise of the interferometer is dominated by the radiation pressure noise. The mirror mass considered here is almost 7 orders of magnitude higher than the measurements reported so far. Our analysis is based on the subsequent observations of the sensitivity curve of Advanced Virgo in different frequency bands (at low and high frequency), for different squeezing quadratures and different levels of injected squeezing. We obtained the data presented in this Letter in two independent measurement campaigns. The first was performed during the preparation phase prior to the third joint Advanced LIGO-Virgo scientific run O3, the second set was carried out during a dedicated break within the science run period. In the same time frame, QRPN has also been observed in the Advanced LIGO detector [16].

Experimental setup.—A sketch of the experimental setup is shown in Fig. 1, and a more detailed description can be found in [8] and references therein. In the following, we briefly summarize the main features. The Advanced Virgo gravitational wave detector is a large-scale, power-recycled Michelson laser interferometer [17] with Fabry-Perot arm cavities. The 42 kg mirrors of the 3 km long arm cavities, the beamsplitter, and the power recycling mirror are all suspended to multistage mechanical filters for seismic noise isolation. The optical gain of the power recycling

Published by the American Physical Society under the terms of the [Creative Commons Attribution 4.0 International license](https://creativecommons.org/licenses/by/4.0/). Further distribution of this work must maintain attribution to the author(s) and the published article's title, journal citation, and DOI.

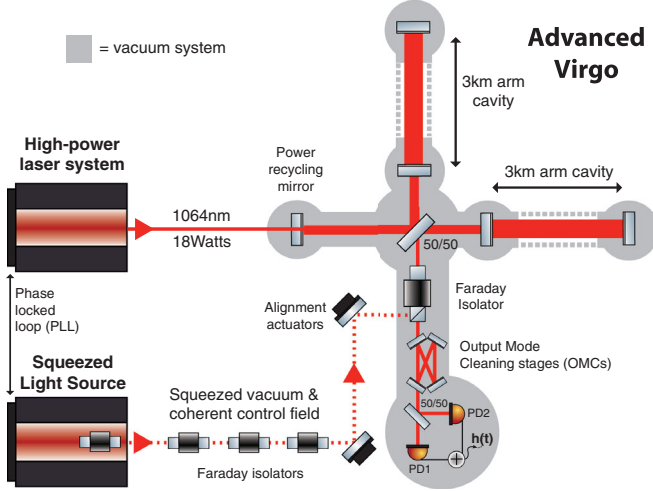


FIG. 1. Simplified layout of the quantum manipulated Advanced Virgo detector as operated during the observational run O3. Advanced Virgo is a power recycled Michelson interferometer using 3 km long Fabry-Perot arm cavities. The interferometer output field is spatially filtered by two output mode cleaning cavities (OMCs), for simplicity drawn as a single stage cavity in the figure and split in two beams before detection. The sum of the two signals from the photodetectors is used to derive the interferometer strain signal $h(t)$. The interferometer main optics and the injection or detection benches are suspended and operated inside a vacuum envelope. Squeezed vacuum states of light are prepared on an external optical bench and are injected into the interferometer after the transmission through a sequence of Faraday isolators.

cavity is 36 and the finesse of the Fabry-Perot arm cavities is 465. A continuous wave laser input power of 18.4 W entering into the interferometer, at a wavelength of 1064 nm, leads to a circulating power of ~ 100 kW inside the arm cavities. The gravitational wave signal is extracted from the antisymmetric port of the Michelson interferometer, where the arms length is kept slightly different to implement the dc-readout scheme [18,19]. This optical field propagates through a Faraday isolator and is subsequently filtered with two optical resonators serving as output mode cleaning stages (OMCs). In transmission and reflection of a 50/50 beamsplitter, the final signal is extracted from the sum of the two photodiodes PD1 and PD2 in Fig. 1. The detection photodiodes and the related optics are placed on suspended benches in vacuum, connected with the interferometer main vacuum system.

The squeezed light source is located on an external optical bench, operated in air. Squeezed vacuum states of light at a wavelength of 1064 nm are generated by means of a doubly resonant optical parametric amplifier (OPA) operated below threshold. The generated squeezing level (squeezing factor) can be tuned with the set point of the intensity stabilization loop of the OPA pump field at the wavelength of 532 nm. More information on the conceptual design of the squeezed light source can be found in [20].

After transmission through a chain of four low-loss Faraday isolators [21], a pair of piezoactuated steering mirrors is used for (automatic) alignment to inject the squeezed field into the interferometer vacuum envelope through an optical window. The interferometer antisymmetric port output field spuriously reflected by the output Faraday isolator towards the squeezing system may eventually be backreflected or backscattered by a moving optics and reenter the interferometer, degrading the sensitivity typically at low-mid frequencies. This effect is suppressed down to a negligible level by a careful design of the optical layout of the squeezing system, the high quality of the optical components, the clean environment, and, for the light back-reflected by the OPA, the combined extinction ratio (approximately 150 dB) of the Faraday isolators [22].

A coherent control scheme [23] is employed to control the phase of the squeezed vacuum field. By choosing appropriate control parameters of this loop, one can inject either squeezing in the phase quadrature (with antisqueezing in the amplitude quadrature) or vice versa, or any linear combination of the two. Squeezing injected in the phase quadrature results in a reduction of QSN and an increase of QRPN, whereas injected squeezing in the amplitude quadrature leads to an increase of QSN and a reduction of QRPN.

Advanced Virgo quantum noise model: In the following, we describe the interferometer sensitivity in terms of test mass displacement noise, i.e., the power spectral density of the product $L \cdot h(t)$, where L is the length of the interferometer arms and $h(t)$ is the strain signal. This represents the differential length change of interferometer arms in the limit of free-falling test masses and in the long wavelength limit for a gravitational wave of optimal polarization and amplitude $h(t)$ at normal incidence on the interferometer plane. The displacement power spectral density can be written as the sum of nonquantum noise and the quantum noise: $S_L(f, \theta, x) = S_{\text{nq}}(f) + S_q(f, \theta, x)$. The nonquantum contribution includes thermal noise and all technical noise sources, for example electronic, laser frequency, and seismic noise. For a power recycled interferometer with squeezed light injection, the quantum noise can be written in terms of the OPA nonlinear strength x ($x = 0$ if no squeezing is applied) and of the squeezing ellipse rotation angle θ [24,25]

$$\begin{aligned}
 S_q(f, \theta, x) = & \alpha_S(f) S_{\text{SN}}(f) \left\{ 1 + \frac{\beta(f)}{\alpha_S(f)} [\mathcal{A}_\theta(x) - 1] \right\} \\
 & + \alpha_R(f) S_{\text{RPN}}(f) \left\{ 1 + \frac{\beta(f)}{\alpha_R(f)} [\mathcal{A}_\theta(x) - 1] \right\} \\
 & + \beta(f) [\mathcal{A}_{\theta-\pi/4}(x) \\
 & - \mathcal{A}_{\theta+\pi/4}(x)] \sqrt{S_{\text{SN}}(f) S_{\text{RPN}}(f)}, \quad (1)
 \end{aligned}$$

where the terms in braces at the first and second line represent the squeezing enhancement factors for QSN and

TABLE I. Advanced Virgo main parameters. The improvement of detection efficiency between the two data taking periods in February and May 2019, though smaller than the systematic uncertainty on ϵ_d , is mainly due to the installation of high quantum efficiency photodiodes.

Parameter	Value
P_{in} —Laser input power	18.4 ± 1 W
G_{pr} —Power recycling cavity gain	36 ± 0.2
M —Mirror mass	42 kg
L —Arm length	3000 m
\mathcal{F} —Arm cavity finesse	465 ± 5
λ —Carrier wavelength	1064 nm
η_i —Squeezing injection efficiency	$(86 \pm 4)\%$
ϵ_c —Arm cavity fractional loss	$(4 \pm 1)\%$
η_d —Detection efficiency (February)	$(65 \pm 11)\%$
η_d —Detection efficiency (May)	$(70 \pm 12)\%$

for QRPN, respectively, and $\mathcal{A}_\theta(x)$ is the squeezing enhancement factor for the lossless interferometer

$$\mathcal{A}_\theta(x) = 1 - 4x \left(\frac{\langle \cos^2 \theta \rangle}{(1+x)^2} - \frac{\langle \sin^2 \theta \rangle}{(1-x)^2} \right), \quad (2)$$

here, terms in brackets are averages over fluctuations of the squeezing angle. A pure phase-squeezed vacuum corresponds to $\theta = 0$, while amplitude-squeezed vacuum corresponds to $\theta = \pi/2$. The QSN and QRPN terms are given by

$$\begin{aligned} S_{\text{SN}}(f) &= \frac{1}{(4\mathcal{F})^2} \cdot \frac{\pi \hbar \lambda c}{P_{\text{bs}}} \cdot \frac{1}{g(f)}; \\ S_{\text{RPN}}(f) &= \left(\frac{4\mathcal{F}}{M} \right)^2 \cdot \frac{\hbar P_{\text{bs}}}{\pi^5 \lambda c} \cdot \frac{g(f)}{f^4}, \end{aligned} \quad (3)$$

and can be calculated using the parameters of the interferometer listed in Table I. The input power on the beamsplitter is $P_{\text{bs}} = P_{\text{in}} \cdot G_{\text{pr}}$ and $g(f) = [1 + (f/f_p)^2]^{-1}$ is the frequency response of the Fabry-Perot arm cavity with pole frequency $f_p = c/4\mathcal{F}L$. The squeezing factors depend on the frequency-dependent loss terms $\alpha_S(f) = 1/\eta_d + \epsilon_c g(f)$, $\alpha_R(f) = 1 + \epsilon_c [1/2 - g(f)]$, and $\beta(f) = [1 - \epsilon_c g(f)]\eta_i$ (see Supplemental Material [26]).

Experimental results.—To provide evidence of quantum radiation pressure noise, we measured the Advanced Virgo detector displacement sensitivity with and without squeezing injection. By manipulating the quantum noise via squeezed vacuum, we can enhance QRPN up to observable levels, and we can subtract the otherwise dominant technical noises with differential measurements. Moreover, the measure of QSN antisqueezing from high-frequency spectra, where shot noise is dominant, provides a precise reference for the expected QRPN enhancement. Data were collected in two sets of measurements in February and May 2019, respectively. In both sets, we varied the OPA

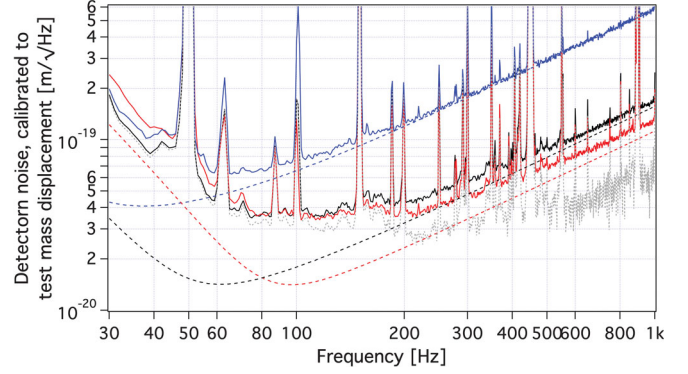


FIG. 2. Displacement sensitivities $\sqrt{S_L}$ as measured in February 2019 and the corresponding quantum noise models $\sqrt{S_q}$ (dashed lines). Black trace: without squeezed vacuum injection. Red trace: with phase-squeezed light injection ($\theta = 0$, $x = 0.66$). Blue trace: with amplitude-squeezed light injection ($\theta = \pi/2$, $x = 0.66$). The gray trace illustrates the total nonquantum noise $\sqrt{S_{\text{ng}}}$. Experimental spectra are calculated from FFT averaged over 300 s time.

nonlinear strength x and the squeezing ellipse rotation angle θ to inject different degrees of phase-squeezed and of amplitude-squeezed vacuum fields.

Figure 2 shows measurements of the detector noise calibrated to test mass displacement as taken in February 2019. The black trace is the measured sensitivity without squeezed light injection. The noise level shown in the red trace is obtained by the injection of a squeezed vacuum field with squeezing in the phase quadrature ($\theta = 0$). The blue trace is the result of the injection of an amplitude quadrature squeezed field ($\theta = \pi/2$). The dashed lines correspond to the quantum noise model for the Advanced Virgo detector as calculated with Eq. (1) and February 2019 parameters, as shown in Table I. Without a squeezed vacuum input ($x = 0$), the model yields the black dashed line. Using Eq. (1) with an OPA nonlinear strength of $x = 0.66$, corresponding to 13.8 dB of generated squeezing, and a rotation angle of $\theta = 0$ and $\theta = \pi/2$ gives the red and blue dashed lines, respectively. The gray trace illustrates the nonquantum noise contributions which explain the deviation between the dashed lines and the corresponding sensitivity measurements. Potential sources of high-frequency technical noise are discussed in [8]. At frequencies above 200 Hz, the detector sensitivity is mainly limited by quantum shot noise with a technical noise clearance ranging from 5 dB at 250 Hz to up of 8 dB in the kHz region. In this frequency window, the sensitivity can be improved via the injection of phase-quadrature squeezed light. In the detection band between 30 and 70 Hz, the corresponding antisqueezing amplifies the effects of quantum radiation pressure noise to an observable level, as suggested from the noise enhancement and as demonstrated with the following analysis. In the unsqueezed interferometer, the direct observation of QRPN would not

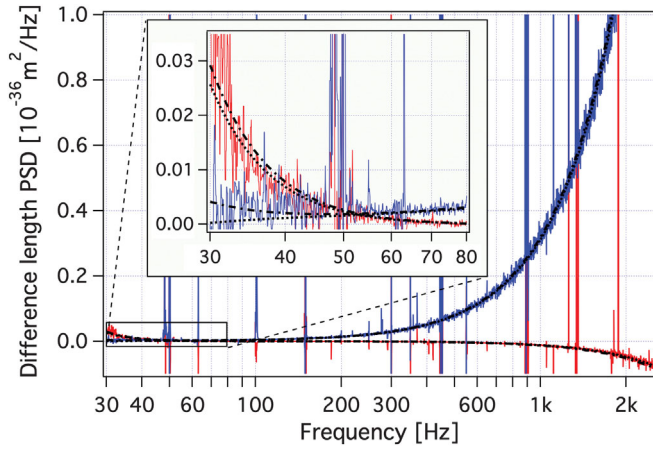


FIG. 3. Power spectral density (PSD) S_{dq} in the presence of phase-squeezed light (red trace) and of amplitude-squeezed light (blue trace) with respect to nonsqueezing; data are calculated from the same data set of Fig. 2. Error bars, not shown on the plot, are about 30% of the S_L value. Black dotted lines represent the quantum noise model, i.e., Eq. (4), estimated from high-frequency phase squeezing and amplitude squeezing; the black dashed-dotted line represents the two-parameters least-squares fit of experimental data with phase squeezing against Eq. (4).

have been possible as this quantum effect is masked by technical noise. It is worth noting that, for the case of amplitude squeezing injection, the enhanced QSN power spectral density is estimated to be larger than the QRPN contribution above 13 Hz. Therefore, the observed noise excess above 30 Hz (blue curve) is mainly due to shot noise contribution.

To demonstrate the observation of QRPN, we analyze the quantum noise in detail, for which one has to remove the technical noise background from measured data, which is especially relevant at low frequencies. Therefore, we use the data shown in Fig. 2 to subtract the unsqueezed displacement power spectrum $S_L(f, 0, 0)$ from the squeezed displacement power spectrum $S_L(f, \theta, x)$ (with $\theta = 0$ or $\pi/2$) to obtain the differential quantum noise

$$\begin{aligned} S_{dq}(f, \theta, x) &= S_L(f, \theta, x) - S_L(f, 0, 0) \\ &= \beta(f) \{ S_{SN}(f) [\mathcal{A}_\theta(x) - 1] \\ &\quad + S_{RPN}(f) [\mathcal{A}_{\theta+\pi/2}(x) - 1] \}, \end{aligned} \quad (4)$$

where the cross-correlation term, i.e., the third line of Eq. (1), has been omitted for simplicity, as it is not relevant if the squeezing angle is a multiple of $\pi/2$. S_{dq} represents the change of quantum noise when injecting squeezed light, and does not depend on nonquantum noise as long as the technical noise is not affected by squeezing injection; this condition is satisfied in our case due to the large value of the optical isolation of the squeezing source. Figure 3 shows S_{dq} for phase squeezing and amplitude squeezing.

The QRPN enhancement due to phase-squeezed light injection is clearly visible at frequencies between 30 and 70 Hz.

According to Eq. (1), both the parameters that factorize the QNRP and QSN contribution in the case of phase and amplitude squeezing, respectively, should depend linearly on $\mathcal{A}_{\pi/2}$. Thus, for each x , we can obtain two independent estimations of the $\mathcal{A}_{\pi/2}$ value, namely $\mathcal{A}_{\pi/2}^{SN}$ from the high frequency part of $S_{dq}(f, \pi/2, x)$, i.e., from data with amplitude squeezing, and $\mathcal{A}_{\pi/2}^{RPN}$ from the low frequency part of $S_{dq}(f, 0, x)$, i.e., from data with phase squeezing. To verify the observation of QRPN, one should find the same values for $\mathcal{A}_{\pi/2}^{RPN}$ and $\mathcal{A}_{\pi/2}^{SN}$. To this purpose, we fit the experimental power spectral density difference S_{dq} for two independent data sets ($\theta = 0$ and $\theta = \pi/2$), excluding major noise peaks, against Eq. (4) with \mathcal{A}_0 and $\mathcal{A}_{\pi/2}$ as free parameters, and $S_{SN}(f)$, $S_{RPN}(f)$ calculated from the parameters of Table I. The data at high frequency, where QSN dominates, provide a precise measurement of the squeezing and antisqueezing factors. Thus, our best model for the quantum noise spectral density in the presence of squeezed light is given by Eq. (4) with the squeezing parameters determined from the high frequency noise spectra, i.e., with $\mathcal{A}_{\pi/2} = \mathcal{A}_{\pi/2}^{SN}$ from the fit of data with amplitude squeezing, and $\mathcal{A}_0 = \mathcal{A}_0^{SN}$ from the fit of data with phase squeezing. The best model is shown in Fig. 3 together with the two-parameter least-squares fit of phase-squeezing data. Model and fit are clearly identical at high frequency; the fair agreement at low frequency for the case of phase squeezing demonstrates that the functional form of our model is compatible with the experimental data and suggests that we can predict the QRPN enhancement from high-frequency noise spectra, as shown in the subsequent analysis. For the case of amplitude squeezing, the trend of low frequency data qualitatively agrees with model's prediction; above 30 Hz, S_{dq} is mostly determined by QSN, i.e., by the $\mathcal{A}_{\pi/2}(x)$ parameter: technical noise fluctuations are much larger than quantum noise, and the squeezing fit parameter $\mathcal{A}_0(x)$ accounting for QRPN contribution, which is, however, unnecessary for the following analysis, is always compatible with zero.

In the quantum model of the interferometer, the squeezing enhancement factors scale with the nonlinear strength x . So in order to prove that the observed low frequency noise enhancement is actually due to QRPN, we compare the antisqueezing factors of QRPN and QSN for different levels of injected squeezing. From Eq. (4), we note that S_{dq} does not depend on detection losses ϵ_d ; moreover, the difference in the common factor $\beta(f)$ of QSN and QRPN terms between high and low frequency is only due to the small contribution of cavity loss ϵ_c . Given the uncertainty on parameters in Table I, the quantum noise model prediction becomes $\mathcal{A}_{\pi/2}^{RPN}[\text{dB}] = 1.0 \cdot \mathcal{A}_{\pi/2}^{SN}[\text{dB}] \pm 1.2$.

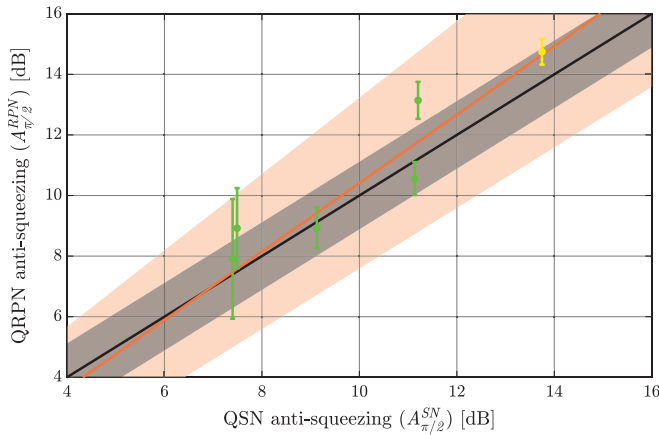


FIG. 4. QRPN antisqueezing factor $A_{\pi/2}^{\text{RPN}}$, measured from low-frequency data with phase squeezing, versus QSN antisqueezing factor measured from high-frequency data with amplitude squeezing. Error bars represent statistical uncertainty, i.e., the standard error in the least-squares fit of experimental spectral data with quantum noise model. Horizontal error bars are not visible on the scale of the plot. The black shaded area indicates the confidence interval for the model, derived from uncertainties presented in Table I. Orange line and shaded area are a linear fit to data and the corresponding 1σ confidence interval. The yellow point corresponds to data presented Fig. 3.

Figure 4 shows the QRPN enhancement factor $\mathcal{A}_{\pi/2}^{\text{RPN}}$ versus the QSN enhancement factor $\mathcal{A}_{\pi/2}^{\text{SN}}$ for six different values of the OPA nonlinear strength, where the error bars are given by the standard uncertainty on the S_{dq} fit with Eq. (4). A linear fit of the experimental data yields $\mathcal{A}_{\pi/2}^{\text{RPN}}[\text{dB}] = (1.1 \pm 0.1) \cdot \mathcal{A}_{\pi/2}^{\text{SN}}[\text{dB}] - (0.9 \pm 1.5)$. The dispersion of data points is affected by nonstationarity of the low frequency technical noise sources. To estimate and mitigate such fluctuations, we acquired an independent $S_L(f, 0, 0)$ reference for each data point in Fig. 4. The reduced χ^2 of the linear fit is 2.8, but it drops to 1.4 when adding to the $\mathcal{A}_{\pi/2}^{\text{RPN}}$ uncertainty the variance of the unsqueezed reference spectra $S_L(f, 0, 0)$ in the 30–70 Hz range. Figure 4 shows confidence intervals for the linear fit of experimental data and for the quantum noise model. Our data are in good agreement with the quantum mechanical interferometer model, and confirm the observation of QRPN.

Conclusion.—Using the Advanced Virgo gravitational wave detector, we were able to extend the observation of QRPN to a yet unexplored regime. By the injection of squeezed vacuum states of light into the dark port of the interferometer, we manipulated the quantum backaction noise to generate a displacement of the 42 kg mirrors measurable at frequencies between 30 and 70 Hz. We showed that the Advanced Virgo detector is operating close to its quantum limit as the effects of QSN and QRPN dominate over most of the detection band when injecting squeezed light with a frequency independent squeezing

angle. The experimental data, obtained in various interferometer configurations, was tested against the Advanced Virgo detector quantum noise model which confirmed the measured magnitude of QRPN. Since the expected reduction of technical noise and the increase of the interferometer laser power will make the QRPN even more dominant, the implementation of backaction evading techniques will be the prerequisite to fully exploit the potential of the squeezed light technique. In this context, the Virgo collaboration is working on the development of a frequency dependent squeezing vacuum source, based on the filter cavity method [25,27,28], which should allow the reduction of quantum noise over the entire detection band [29]. In comparison to previous QRPN experiments at room temperature, the free-mass oscillator reported here is almost 7 orders of magnitude heavier and the observation frequencies could be lowered by a factor of 10. This so far unexplored parameter range might offer new opportunities for fundamental physics, for example, to explore the transition between quantum and classical worlds, investigate gravity-induced decoherence, or phenomenological quantum gravity [30,31].

The authors gratefully acknowledge the support of the Max Planck Society, Leibniz Universität Hannover, and Deutsche Forschungsgemeinschaft (DFG, German Research Foundation) through Grant No. VA 1031/1-1 and Germany’s Excellence Strategy Grant No. EXC-2123 QuantumFrontiers—390837967 for the construction, installation, and operation of the squeezed light source. The authors gratefully acknowledge the Italian Istituto Nazionale di Fisica Nucleare (INFN), the French Centre National de la Recherche Scientifique (CNRS), and the Netherlands Organization for Scientific Research, for the construction and operation of the Virgo detector and the creation and support of the EGO consortium. The authors also gratefully acknowledge research support from these agencies as well as by the Spanish Agencia Estatal de Investigación, the Conselleria d’Innovació, Universitat, Ciència i Societat Digital de la Generalitat Valenciana and the CERCA Programme Generalitat de Catalunya, Spain, the National Science Centre of Poland, the European Commission, the Hungarian Scientific Research Fund (OTKA), the French Lyon Institute of Origins (LIO), the Belgian Fonds de la Recherche Scientifique (FRS-FNRS), Actions de Recherche Concertées (ARC), and Fonds Wetenschappelijk Onderzoek Vlaanderen (FWO), Belgium. Finally the authors kindly thank S. Danilishin for useful discussions on the quantum noise model of the interferometer.

-
- [1] F. Acernese *et al.* (Virgo Collaboration), *Classical Quantum Gravity* **32**, 024001 (2015).
 - [2] J. Aasi *et al.* (LIGO Scientific Collaboration), *Classical Quantum Gravity* **32**, 115012 (2015).

- [3] K. L. Dooley *et al.*, *Classical Quantum Gravity* **33**, 075009 (2016).
- [4] Y. Aso, Y. Michimura, K. Somiya, M. Ando, O. Miyakawa, T. Sekiguchi, D. Tatsumi, H. Yamamoto, *Phys. Rev. D* **88**, 043007 (2013).
- [5] V. B. Braginsky, *Zh. Eksp. Teor. Fiz.* **53**, 1434 (1967).
- [6] C. M. Caves, *Phys. Rev. D* **23**, 1693 (1981).
- [7] H. Grote, K. Danzmann, K. L. Dooley, R. Schnabel, J. Slutsky, and H. Vahlbruch, *Phys. Rev. Lett.* **110**, 181101 (2013).
- [8] F. Acernese *et al.* (Virgo Collaboration), *Phys. Rev. Lett.* **123**, 231108 (2019).
- [9] M. Tse *et al.*, *Phys. Rev. Lett.* **123**, 231107 (2019).
- [10] T. P. Purdy, R. W. Peterson, and C. A. Regal, *Science* **339**, 801 (2013).
- [11] J. D. Teufel, F. Lecocq, and R. W. Simmonds, *Phys. Rev. Lett.* **116**, 013602 (2016).
- [12] M. Rossi, D. Mason, J. Chen, Y. Tsaturyan, and A. Schliesser, *Nature (London)* **563**, 53 (2018).
- [13] J. Cripe, N. Aggarwal, R. Lanza, A. Libson, R. Singh, P. Heu, D. Follman, G. D. Cole, N. Mavalvala, and T. Corbitt, *Nature (London)* **568**, 364 (2019).
- [14] J. B. Clark, F. Lecocq, R. W. Simmonds, J. Aumentado, and J. D. Teufel, *Nat. Phys.* **12**, 683 (2016).
- [15] M. J. Yap *et al.*, *Nat. Photonics* **14**, 19 (2020).
- [16] H. Yu *et al.*, *Nature (London)* **583**, 43 (2020).
- [17] R. W. P. Drever, *Gravitational Radiation* (North-Holland, Amsterdam, 1983).
- [18] S. Hild *et al.*, *Classical Quantum Gravity* **26**, 055012 (2009).
- [19] T. T. Fricke *et al.*, *Classical Quantum Gravity* **29**, 065005 (2012).
- [20] M. Mehmet and H. Vahlbruch, *Classical Quantum Gravity* **36**, 015014 (2019).
- [21] E. Genin, M. Mantovani, G. Pillant, C. De Rossi, L. Pinard, C. Michel, M. Gosselin, and J. Casanueva, *Appl. Opt.* **57**, 9705 (2018).
- [22] AdV Squeezing Working Group, Virgo-Technical Documentation System VIR-0761B-17, <https://tds.virgo-gw.eu/?content=3&r=13905> (2017).
- [23] H. Vahlbruch, S. Chelkowski, B. Hage, A. Franzen, K. Danzmann, and R. Schnabel, *Phys. Rev. Lett.* **97**, 011101 (2006).
- [24] S. E. Dwyer, Ph.D. thesis, Massachusetts Institute of Technology, 2013.
- [25] H. J. Kimble, Y. Levin, A. B. Matsko, K. S. Thorne, and S. P. Vyatchanin, *Phys. Rev. D* **65**, 022002 (2001).
- [26] See Supplemental Material at <http://link.aps.org/supplemental/10.1103/PhysRevLett.125.131101> for a derivation of the quantum noise model leading to Eq. (1).
- [27] Y. Zhao *et al.*, *Phys. Rev. Lett.* **124**, 171101 (2020).
- [28] L. McCuller *et al.*, *Phys. Rev. Lett.* **124**, 171102 (2020).
- [29] The Virgo Collaboration, Virgo-Technical Documentation System, Report No. VIR-0596A-19, 2019.
- [30] A. Bassi, K. Lochan, S. Satin, T. P. Singh, and H. Ulbricht, *Rev. Mod. Phys.* **85**, 471 (2013).
- [31] Y. Chen, *J. Phys. B* **46**, 104001 (2013).